# Efficiency of Volatile Corrosion Inhibitors in the Presence of n-Heptane: An Experimental and Molecular Simulation Study

Maryam Eslami, \*\*\*\* Sumit Sharma, \* David Young, \* and Marc Singer \*

Volatile corrosion inhibitors (VCIs), specifically formulations based on thiols and amines, can be used to mitigate top-of-the-line corrosion (TLC) that arises during the transportation of wet gas through transmission pipelines. Nevertheless, the VCI inhibition efficiency (IE) can be compromised by the presence of condensable hydrocarbon phases. In this research, the IE of two thiol compounds (decanethiol and hexanethiol) and three combinations of VCIs for TLC scenarios, both in the presence and absence of n-heptane, representing a condensing hydrocarbon phase were studied. The results proved the IE of thiols in a water-only condensing environment, with effectiveness increasing with the alkyl tail length. Conversely, in a water/n-heptane co-condensing environment, a reversed trend was observed, where hexanethiol exhibited higher corrosion IE compared to decanethiol. Molecular simulation results indicated a synergistic adsorption behavior when the alkane was of a similar length as the alkyl tails of the inhibitors, leading to the incorporation of alkane molecules with the inhibitor molecules. A mixture of thiols (decanethiol and hexanethiol) and two mixtures of thiol and amines (decanethiol and diethylamine/t-butylamine) were also considered in both water-only and water/n-heptane co-condensing environments. In the presence of n-heptane, only the thiol mixture, featuring molecules with different tail lengths, demonstrated high IE. This behavior was attributed to the superior IE provided by thiol-based molecules with a shorter alkyl tail (hexanethiol) in the presence of n-heptane. Additionally, the results revealed that the mixtures of decanethiol and amines did not enhance corrosion inhibition in the presence of n-heptane within the system.

KEY WORDS: CO<sub>2</sub> corrosion, hydrocarbons, n-heptane, top of the line corrosion, volatile corrosion inhibitors

## INTRODUCTION

The mode of corrosion referred to as top-of-the-line (TLC) is a phenomenon observed during the transportation of wet gas. It arises from temperature variations between pipelines and their surroundings, causing water condensation and subsequent deterioration of metal. This corrosion occurs due to the condensation of saturated vapors present in the unprocessed gas stream, which accumulates on the inner surface of the cold pipe wall. The resulting condensed liquid comprises hydrocarbons and water, forming a thin film and/or droplets on the pipeline. Initially, this condensed water phase can be highly corrosive to standard carbon steel pipelines because it contains dissolved acid gases (such as carbon dioxide [CO<sub>2</sub>], hydrogen sulfide [H<sub>2</sub>S]) and organic acids (e.g., acetic acid [CH<sub>3</sub>COOH]). <sup>1-2</sup>

The mechanism of sweet TLC is similar to what takes place in the bulk liquid phase.<sup>3</sup> Nevertheless, TLC presents distinctive characteristics that pose challenges for mitigation and increase the likelihood of localized corrosion. The occurrence of TLC is influenced by factors such as fluid temperature, flow regime, water condensation rate (WCR), CO<sub>2</sub>/H<sub>2</sub>S content, and organic acid concentration.<sup>1</sup> The initial rate of uniform corrosion is relatively high, however, it diminishes over time as ferrous ions are released into the condensed water, leading to a subsequent rise in pH. Once the saturation

point of ferrous ions in the condensed water is attained (depending on the system temperature), the precipitation of a corrosion product layer (FeCO $_3$ ) takes place. From a thermodynamic perspective, precipitation of FeCO $_3$  occurs when the saturation level ( $S_{FeCO}_3 = [Fe^{2+}][CO_3^2-]/K_{sp,FeCO}_3$ ) exceeds one. In the mentioned equation,  $K_{sp,FeCO}_3$  is the solubility product, which is a function of temperature and ionic strength. The formed FeCO $_3$  layer has the potential to be protective against corrosion. In the course of TLC process, freshly condensed water, devoid of ferrous ions, continues to dilute the existing electrolyte. As the chemistry of the solution undergoes continuous changes, the protectiveness of the FeCO $_3$  layer is constantly challenged leading to inescapability of localized corrosion, although to a variable extent.  $^1$ 

In stratified flow regimes (that are favorable for TLC to occur), conventional CO<sub>2</sub> corrosion inhibitors are impractical to protect the top-of-the-line because they are only in contact with the bottom of the pipe (where the liquid phase is in contact with the metal surface) and will not reach the upper surface of the pipe. Therefore, in order to combat TLC other strategies such as batch corrosion inhibition (BCI) using pigging technology have been applied. PBCI treatment requires operational shutdowns that lead to massive production losses, moreover, not all of the pipelines in service are compatible with pigging technology.

Submitted for publication: January 29, 2024. Revised and accepted: April 08, 2024. Preprint available online: April 10, 2024, https://doi.org/10.5006/4531.

<sup>&</sup>lt;sup>‡</sup> Corresponding author. E-mail: meslami@illinois.edu.

<sup>\*</sup> Institute for Corrosion and Multiphase Technology, Department of Chemical and Biomolecular Engineering, Ohio University, Athens, Ohio 45701.

<sup>\*\*</sup> Applied Research Institute, University of Illinois Urbana-Champaign, Champaign, Illinois 61820.

Table 1. Nominal Composition of UNS G10180 Carbon Steel Specimens											
	С	Mn	Р	s	Nb	Cr	Ni	Мо	Cu	Al	Fe
Composition (wt%)	0.17	0.66	0.007	0.02	0.002	0.073	0.06	0.04	0.14	0.04	Balance

Another viable method is the use of volatile corrosion inhibitors (VCI) to mitigate corrosion of equipment parts exposed to the vapor phase. 11-14 VCIs are organic compounds usually with a high vapor pressure. When applied to the system, the VCI reaches the metal surface through the gas phase and condenses to form a thin film, rendering the surface relatively passive. This film separates the metal from the corrosive environment. The mitigation provided by VCIs depends on the nature and surface charge of the metal, type of aggressive media present, structures of inhibitor molecules, and molecular interactions at the metal surface. 15 As an example, when the steel surface carries a positive charge (vs. the potential of zero charge) and the VCI is an alkanethiol, the interaction between the permanent dipole of the thiol head group (R-SH with a partial negative charge on the sulfur [S] atom) and the steel surface is expected to be favored, leading to adsorption through electrostatic interaction. The inhibition mechanism by VCIs is electrochemical mirroring the electrochemical nature of the corrosion process itself, a fact substantiated by various studies.<sup>14</sup> For instance, the potentiodynamic polarization measurements on X65 steel in CO2 saturated 1 wt% NaCl solution in the presence of 5 ppm<sub>v</sub> to 400 ppm<sub>v</sub> decanethiol have revealed a deceleration of both anodic and cathodic reactions in the charge transfer-controlled regions of the polarization curves. 15 Others have reported similar findings, and it is crucial to highlight that inhibition can be primarily anodic, cathodic, or a combination of both. 16-18

The common VCIs used incorporate functionalities such as amine, imine, amide, and thiol. For application in TLC mitigation, achieving the right balance between volatility and inhibition efficiency (IE) is intricate. Determining the optimal functional group, that dictates the adsorption mechanism, and the right length of the alkyl tail pose challenges as well. For instance, to attain a relatively high vapor pressure, ensuring the inhibitor transport to the top-of-the-line, the compound should have a low molecular weight. However, compounds with low molecular weight often exhibit inferior corrosion inhibition.<sup>6</sup>

Despite the mentioned challenges, research on the application of alkanethiol<sup>4,19-24</sup> and amine<sup>17,25-28</sup> model compounds applied for corrosion mitigation of various metals including steel and copper have shown encouraging results.

Based on previous research, 4,15,29-30 decanethiol is an effective model VCI and can significantly reduce localized and uniform TLC of carbon steel under sweet and sour conditions. Under the studied experimental conditions, decanethiol, in particular, and other thiols such as hexanethiol demonstrated greater efficacy compared to alternative inhibitors such as diethylamine in reducing the corrosion rate. This occurs because the amines are predominantly protonated within the tested pH range (3.8 to 5.3). Consequently, their vapor pressure, and subsequently their concentration in the condensed

water, is minimal, preventing them from offering substantial inhibition.<sup>26</sup> Accordingly, the role of amines can be described as limited to adjusting the pH of the condensed water.<sup>27,31</sup>

One of the challenges associated with TLC mitigation is the interference of hydrocarbons with VCI inhibition. In cocondensing environments, hydrocarbons usually form a film covering the surface due to their low surface tension and separate water or liquids with higher surface tension into smaller droplets. Nevertheless, the surface remains hydrophilic, attracting water, and the corrosion process occurs unhindered. In the presence of a hydrocarbon phase such as n-heptane, some effective VCIs such as decanethiol lose their IE and show very poor persistency. Ale This has been attributed to the partitioning of the VCI in the hydrocarbon phase due to its higher solubility in this phase and its lower solubility in water. The available studies to address this interference for different VCIs are limited.

The objective of this research is to compare corrosion inhibition by two different thiols in a water/n-heptane co-condensing environment using experimental and simulation studies. Moreover, the potential synergistic effect of VCI mixtures (thiols and amines) is also investigated in hydrocarbon-containing environments.

## MATERIALS AND METHODS

## 2.1 | Setup and Test Matrix

1018 (UNS G10180<sup>(1)</sup>) steel specimens with a ferritic-pearlitic microstructure were used for the experiments.

The nominal composition of this steel was provided in Table 1.

The steel specimens were machined into a cylindrical shape, with a diameter of 3.15 cm and a height of 1.15 cm. One of the faces and sides of the specimen were covered with Xylan<sup>®†</sup> coating, leaving an exposed area of around 7.8 cm<sup>2</sup>. The exposed surface was subsequently polished up to #600 grit using silicon carbide abrasive papers. They were then ultrasonically cleaned in isopropanol for 5 min and dried.

The experimental setup was a 4 L glass cell especially designed for TLC experiments, as depicted in Figure 1. 2.5 L volume of deionized (DI) water was poured into the glass cell and sparged with  $\mathrm{CO}_2$  for at least 2 h to facilitate deoxygenation and electrolyte saturation. In the experiments that included n-heptane, the volume of DI water was reduced to 1.7 L and 0.8 L of n-heptane was added to the glass cell after the minimum 2 h period of  $\mathrm{CO}_2$  sparging. In this case, sparging was continued for another hour to purge any remaining oxygen from the system and guarantee  $\mathrm{CO}_2$  saturation.

During  $\mathrm{CO}_2$  sparging, the solution was heated to 75°C, using a hot plate, which led the gas temperature to reach ca. 65°C. Evaporation was minimized using a condenser on top of the glass cell setup (Figure 1). After the desired solution temperature was reached, 600 ppm $_{\mathrm{V}}$  of acetic acid and 400 ppm $_{\mathrm{V}}$  of each of the selected inhibitor(s) were added to the solution. The specimen (referred to as weight loss [WL] specimen in Figure 1) was subsequently inserted into the lid, being flush-mounted to its underside; thereby exposing its polished surface to the wet gas phase. To control the WCR, the specimen

<sup>(1)</sup> UNS numbers are listed in Metals & Alloys in the Unified Numbering System, published by the Society of Automotive Engineers (SAE International) and cosponsored by ASTM International.

<sup>&</sup>lt;sup>†</sup> Trade name.

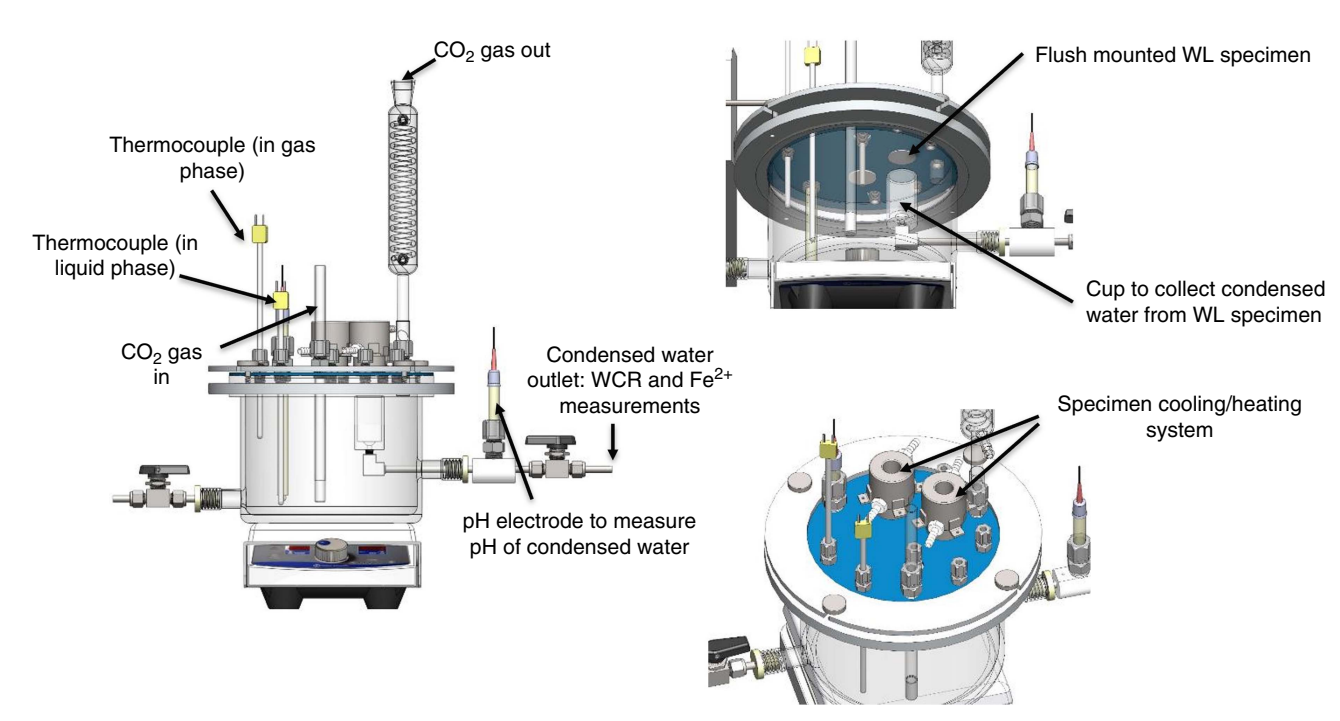


FIGURE 1. The glass cell setup for the TLC experiments.

was cooled to 56°C by circulating water through a heating/ cooling system. The WCR was 0.48±0.04 mL/m<sup>2</sup>/s under this condition. This rate was calculated by measuring the volume of the condensed water accumulated in the cup that was placed underneath the specimen during the experiment (see Figure 1). In the presence of n-heptane, all other conditions being the same, a significant amount of the heat is used to condense the hydrocarbon, leading to a substantial decrease in the WCR. Moreover, it was difficult to reach and maintain the target gas temperature of 65°C, probably due to the different thermal properties of n-heptane compared to water. Consequently, the gas phase temperature in the presence of n-heptane dropped from ca. 65°C to ca. 52°C. Prior works in similar environments have demonstrated that the n-heptane condensation rate is roughly seven times higher than water.32 Under the experimental conditions of this study, it can be anticipated that the WCR would decrease to 0.12 mL/m<sup>2</sup>/s in the presence of nheptane (from 0.48 mL/m<sup>2</sup>/s in the absence of n-heptane). The nheptane condensation rate is estimated at 0.62 mL/m<sup>2</sup>/s. In addition, the partial pressure of CO2, in the experiments with nheptane, would also be lower than those without (ca. 0.74 bar for pure water experiments vs. ca. 0.54 bar for the experiments with water and n-heptane, based on the gas temperature). These considerations point to the lower corrosiveness in environments containing n-heptane, as compared with the pure water systems.

The test matrix is summarized in Table 2. The temperature of the gas, the solution, and the steel specimen were monitored during the experiment. Each experiment was 3 d long. All chemicals used in this study were of analytical grade. All experiments were repeated at least twice.

# 2.2 | Postexperiment Characterization

After each experiment, the corrosion products on the corroded specimens were removed using Clarke solution, according to ASTM Standard G1-03.<sup>33</sup> The specimens were

then rinsed with DI water followed by isopropanol rinsing and subsequently dried with nitrogen ( $N_2$ ). The corrosion rate was calculated using the difference between the initial and the final weight of each specimen before the experiment and after the Clarke solution cleaning. The following equation was used<sup>34</sup>

$$CR = 87,600\Delta m/\rho At$$
 (1)

In this equation, CR is the corrosion rate (mm/y),  $\Delta$ m is the mass difference (g),  $\rho$  is the density of carbon steel (7.874 g/cm³), A is the exposed area (cm²), t is the immersion time (h), and 87,600 is the conversion factor. In addition to the corrosion rate obtained from the WL measurements, the maximum penetration rate for each specimen was determined using optical profilometry data of the maximum penetration depth and a simple proportion calculation. This maximum penetration rate can be used to quantify the extent of localized corrosion:

- If the maximum penetration rate is higher than the average corrosion rate (typically with an arbitrary factor of 5), localized corrosion is likely occurring.<sup>35</sup>
- If the maximum penetration rate is lower than the average corrosion rate, then the specimen suffers from uniform corrosion and the maximum penetration rate is just a representation of surface roughness.

After the corrosion experiments (before and after Clarke solution cleaning), surfaces of the specimens were characterized using scanning electron microscopy (SEM, JEOL JSM-6090 $^{\dagger}$ ), energy dispersive x-ray spectroscopy (EDS, Bruker QUANTAX 400 $^{\dagger}$ ), and optical profilometry (Alicona, IFM $^{\dagger}$ ).

## **MOLECULAR SIMULATIONS**

# 3.1 | Model Description

Molecular simulations were performed to understand the synergistic adsorption of inhibitors in the presence of hydrocarbons/alkanes. A coarse-grained description of the inhibitors and the alkane molecules was used as described in our

Table 2. Test Matrix of Glass Cell Experiments (the Concentration of Acetic Acid was 600 ppm <sub>v</sub> in All Experiments)							
Test ID	Decanethiol (ppm <sub>v</sub> )	Hexanethiol (ppm <sub>v</sub> )	Diethylamine (ppm <sub>v</sub> )	t-Butylamine (ppm <sub>v</sub> )	n-Heptane (L)		
В	0	0	0	0	0		
В-Нер	0	0	0	0	0.8		
D	400	0	0	0	0		
D-Hep	400	0	0	0	0.8		
Н	0	400	0	0	0		
Н-Нер	0	400	0	0	0.8		
D-H	400	400	0	0	0		
D-H-Hep	400	400	0	0	0.8		
D-Di	400	0	400	0	0		
D-Di-Hep	400	0	400	0	0.8		
D-t-B	400	0	0	400	0		
D-t-B-Hep	400	0	0	400	0.8		

<sup>&</sup>lt;sup>(A)</sup> Note: B, blank; D, decanethiol ( $C_{10}H_{22}S$ ); Di, diethylamine ( $C_4H_{11}N$ ); H, hexanethiol ( $C_6H_{14}S$ ); Hep, n-heptane ( $C_7H_{16}$ ); and t-B, t-butylamine ( $C_4H_{11}N$ ).

previous work.<sup>36</sup> In a coarse-grained description, a group of atoms are lumped together into a bead. In this model, an inhibitor molecule is represented by a linear chain of 20 coarse-grained beads, with the first bead as the polar head group and the remaining beads representing the alkyl groups. Alkane molecules are represented by a linear chain of the beads representing the alkyl groups. In the aqueous environment, alkyl beads experience hydrophobic interactions between themselves. These interactions are represented by the Lennard-Jones (LJ) potential function

$$V_{LJ}(r) = 4\varepsilon \left(\frac{\sigma^{12}}{r^{12}} - \frac{\sigma^6}{r^6}\right)$$
 (2)

Equation (2) represents the potential energy between two alkyl beads at a distance r from each other.  $\sigma$  and  $\epsilon$  are the LJ parameters with units of length and energy, respectively.  $\sigma$  can be thought of as a measure of size of the bead and  $\epsilon$  represents the strength of the interaction. Force between the beads is the negative gradient of  $V_{\text{LJ}}(r)$ . The LJ force is repulsive at small distances, which disallows spatial overlaps of the beads, but is attractive at larger distances. The interactions between the polar bead and the metal surface are represented by the 9–3 potential

$$V_{9-3}(z) = \varepsilon_S \left( \frac{2}{15} \frac{\sigma_s^9}{z^9} - \frac{\sigma_s^3}{z^3} \right)$$
 (3)

In this equation, z is the distance of the polar group from the surface,  $\sigma_s$  and  $\epsilon_s$  are length and energy parameters, respectively. The functional form of  $V_{9-3}(z)$  is obtained if one calculates the net interaction of a semi-infinite slab of LJ beads arranged in a solid lattice arrangement. The alkyl beads do not have any attractive interactions with the surface but are not allowed to penetrate the surface. The interactions between the polar head and the alkyl beads are represented by the repulsive part of the LJ interactions. Within a molecule, bonds between adjacent beads are represented by a harmonic potential function, that is,  $V_{bond}(b) = k_{bond}(b-b_o)^2$ , where  $k_{bond}$  is the force constant,  $b_o$  is the equilibrium bond length, and b is the bond length

at any time instant. The molecules are kept linear in shape by applying a harmonic angle potential between three adjacent beads. Water molecules are not included in this coarse-grained description. The effect of water is incorporated by performing Langevin or Brownian dynamics simulation. In a Langevin/Brownian dynamics simulation, a drag force in the direction opposite of the current velocity and proportional to the magnitude of the velocity is applied to each bead. In addition, a Gaussian random force is applied to each bead, which mimics the random collisions between the solvent molecules and the bead. This coarse-grained model has been used in many previous works. <sup>36-39</sup>

In the simulations, the energy is represented in units of  $k_BT$ , where T is the temperature and  $k_B$  is Boltzmann constant.  $\epsilon$  is set to 0.065  $k_BT$  to make the overall hydrophobic interactions between the alkyl tails to approximately 1  $k_BT$ . The strong interaction between the polar group and the metal surface is represented by  $\epsilon_s$  = 5  $k_BT$ . The polar group is considered twice as large as the alkyl bead,  $\sigma_s$  = 2 $\sigma$ . The unit of length is set as  $\sigma$ . The unit of time is  $\sigma(m/k_BT)^{1/2}$ . Considering  $\sigma\sim0.3$  nm, m  $\sim12$  atomic mass units, and room temperature, the unit of time becomes 0.7 ps. In reduced units, the integration timestep is 0.001 ( $\sim\!0.7$  fs) and the Langevin dynamics damping coefficient is taken as 0.1 ( $\sim\!0.07$  ps).

# 3.2 | Simulation Details

The simulation box has the dimensions of  $26.93~\sigma \times 26.94~\sigma \times 80~\sigma$  and has 400 inhibitor and 400 alkane molecules. In real systems, corrosion inhibitor molecules, when first introduced in the system, diffuse toward metal surfaces to adsorb. Upon reaching equilibrium, the local concentration of the molecules near the surface is much higher than in the bulk aqueous phase. Attaining such an equilibrium takes some minutes to hours. However, molecular simulations can only access small timescales (nanoseconds to microseconds). Therefore, to reduce the diffusion time, we use higher concentrations. The number of corrosion inhibitor molecules (400) in the system were chosen so that there are sufficient number of molecules that can cover the entire adsorbing surface. The

<sup>(</sup>B) All concentrations are based on total liquid volume.

number of alkane molecules were chosen to be the same so that there are enough available to observe the possible synergistic adsorption behavior. Initial configurations of the simulation are generated by randomly placing the molecules within the simulation box while ensuring that no two molecules overlap each other. The z = 0 plane represents the metal surface. The plane opposite the metal surface is a reflective, noninteracting plane to keep the system volume constant. The simulation box is periodic in the x and y directions. Our goal is to study the synergistic adsorption behavior of inhibitors in the presence of alkane molecules. The working hypothesis is that the overall adsorption is enhanced when the alkyl tail of the inhibitor matches the length of the alkane. The rationale is the following: if the alkanes are smaller than the alkyl tail of the inhibitor, then the alkanes will disrupt the hydrophobic interactions between the alkyl tails, resulting in less adsorption. On the other hand, when the alkanes are longer than the alkyl tails, then the inhibitors prefer to aggregate with the alkanes in the bulk phase rather than adsorbing on the surface. This hypothesis aligns with the improvement observed in the corrosion IE of hexanethiols in the presence of n-heptane that will be presented in the Results and Discussion section. Therefore, in our simulations, three different alkane lengths: 10 bead long (short), 19 bead long (commensurate with the alkyl tail of the inhibitor), and 25 bead long (long) were studied. The inhibitor molecule is 20 bead long with the first bead representing the polar head and the remaining 19 beads representing the alkyl tail. The simulations are performed in the canonical ensemble (constant number of particles, temperature, and volume). Equilibration is understood to be achieved when the ensemble-averaged number of

adsorbed molecules does not change with time. The self-assembly of adsorbed molecules in organized structures is a slow process in molecular timescales. Equilibration takes  $5 \times 10^8$  molecular dynamics (MD) steps, which is followed by production runs of  $2 \times 10^8$  MD steps. All simulations are performed using the large-scale atomic/molecular massively parallel simulator (LAMMPS) molecular simulations package.

### RESULTS AND DISCUSSION

Corrosion and maximum penetration rates corresponding to the initial six TLC experiments (as outlined in Table 2) are depicted in Figure 2.

Table 3 summarizes the results of IE for decanethiol and hexanethiol in the presence and absence of n-heptane. The IE was calculated using the following equation

$$IE(\%) = \frac{CR(blank) - CR(inhibited)}{CR(blank)} \times 100$$
 (4)

Regarding the blank experiments (i.e., the experiments without inhibitors), the bar chart in Figure 2 shows that the presence of the hydrocarbon phase (n-heptane) decreased the average corrosion rate. However, this conclusion requires further clarification. As mentioned earlier, the condensing environment is significantly less corrosive in the presence of the hydrocarbon phase due to lower WCR and lower pCO<sub>2</sub>. The simulated uniform TLC rate in a water-only environment at a lower WCR (ca. 0.12 mL/m²/s) and at a lower pCO<sub>2</sub> using TOPCORP™† package should be ca. 0.43 mm/y. This means that

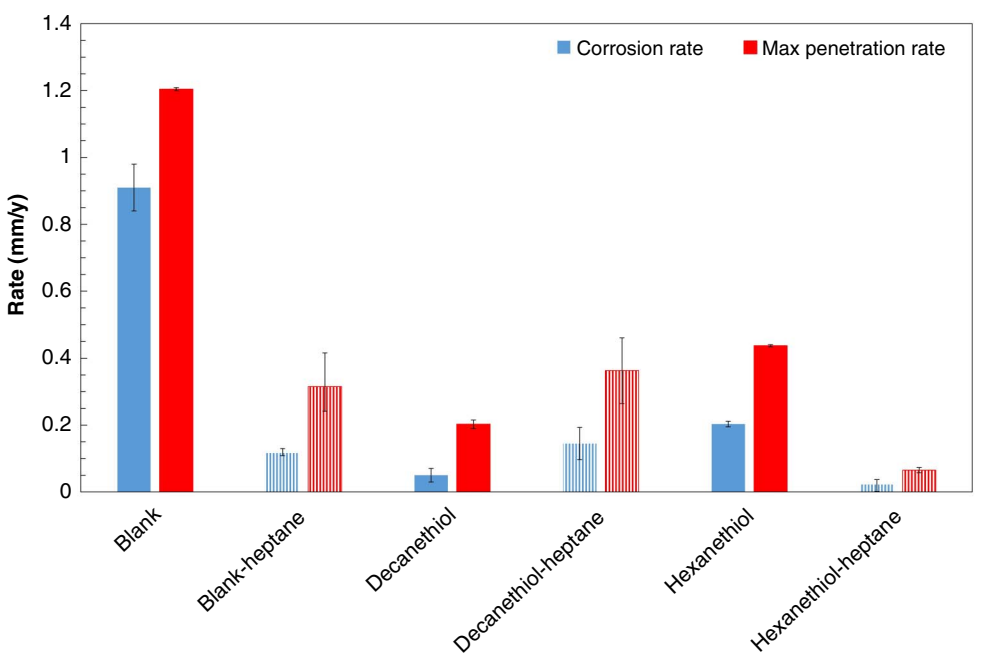


FIGURE 2. Uniform and localized TLC rate for different experiments (the error bars represent maximum and minimum values).

Table 3. IE for Decanethiol and Hexanethiol in Water-Only and Co-Condensing Environment of Water and n-Heptane								
Decanethiol/Water			Decanethiol/Water- Heptane	Hexanethiol/Water	Hexanethiol/Water- Heptane			
IE (%)		94.5	0	77.6	81			

regardless of the decrease in the average corrosion rate, according to Figure 2 at this condition (B-Hep) the maximum penetration rate was similar to the simulated TLC rate in a water-only environment at the same WCR. The decrease in the average corrosion rate in the presence of a condensable hydrocarbon phase, such as n-heptane, can also be attributed to the change in the water wetting of the steel surface or to the change in the water chemistry of the system, this will be explained more with the surface characterization results.

According to a study by Pojtanabuntoeng, et al., 41 in a hydrocarbon-free system, the corrosive condensed water wets the entire surface and the TLC rate increases with the WCR. However, in the presence of n-heptane, alkane molecules wet part of the surface resulting in the segregation of water droplets. In such scenarios, the change in the water droplet chemistry can lead to a rapid formation of FeCO<sub>3</sub>. A corroborating observation was noticed on the steel surface after the blank test with heptane (B-Hep). As can be seen in SEM images in Figure 3(b) at low magnification traces of water droplets on the surface are visible, and at higher magnification (the inserted image in Figure 3[b]) crystals

of FeCO<sub>3</sub> of different morphologies<sup>42</sup> are observed forming a layer on the surface. The areas between the water droplets were wet by n-heptane which, due to its low surface tension on the solid surface, tends to condense in a film-wise manner.<sup>5</sup> More importantly, these surface areas covered by the condensed n-heptane were protected from corrosion, while the areas wet by the aggressive condensed water experienced a higher rate of corrosion. As mentioned above, this was evidenced in similar maximum penetration rate in experiments B-Hep and the TLC rate in a water-only environment at similar condensation rate.

It is noted that according to Figure 2, the maximum penetration rate results do not meet the arbitrary factor of 5 that is usually used to assess the risk of localized corrosion. However, considering the short experiment duration in this research (because the focus was on "inhibition efficiency" rather than the "persistency of inhibitor"), low rates of penetration were expected. Therefore, the reported data could indicate pitting initiation and longer-term experiments would be needed to confirm sustained localized corrosion. It should be mentioned that reporting the maximum penetration rate in this study was merely to compare the IE of different inhibitors in the selected

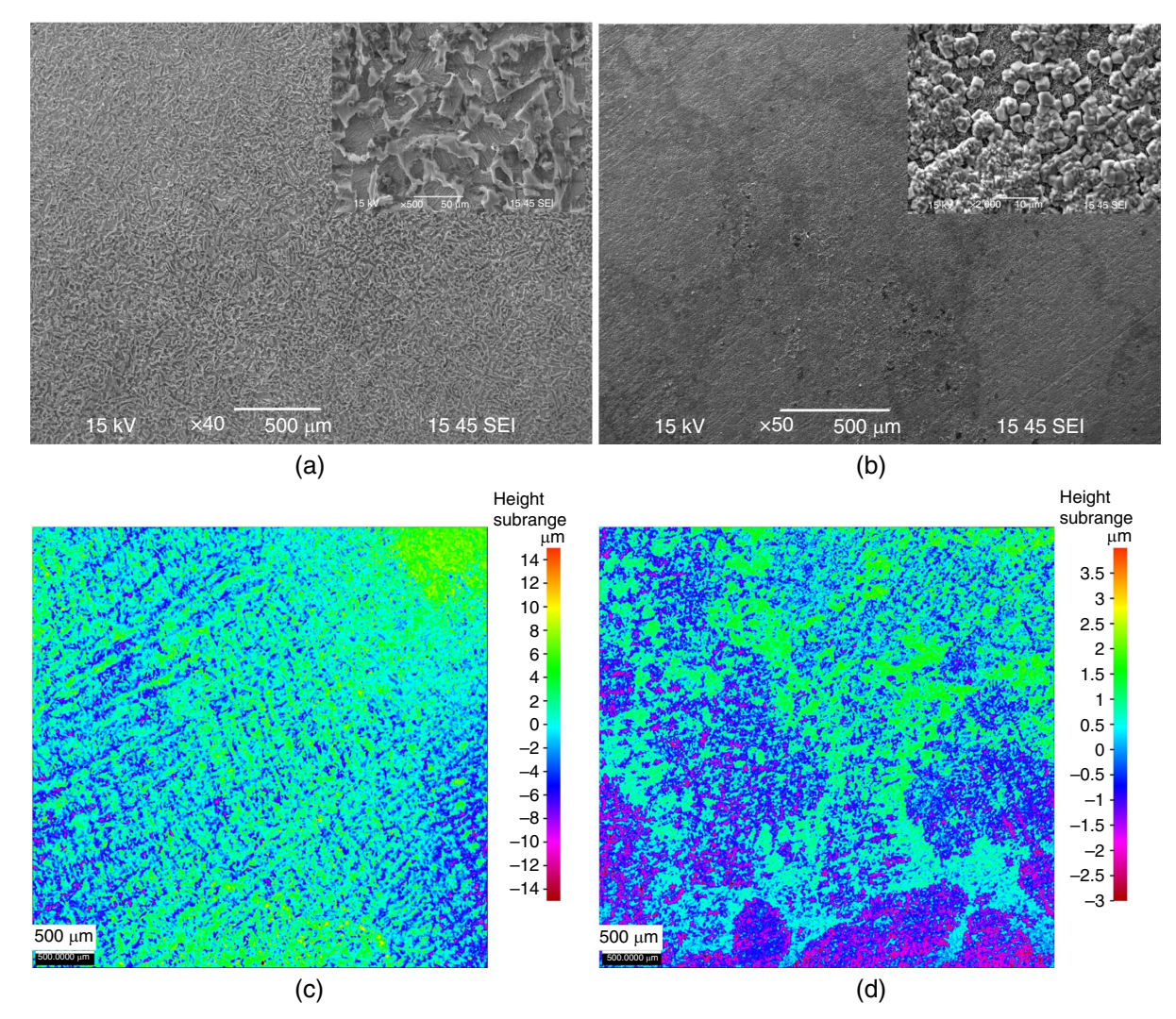


**FIGURE 3.** SEM images of the specimen after the blank experiment: (a) without n-heptane (B) and (b) with n-heptane (B-Hep). Optical profilometry analysis of the specimen after the blank experiment: (c) without n-heptane (B) and (d) with n-heptane (B-Hep).

environments. Longer-term experiences are needed to study both persistency of inhibitors and the localized corrosion rates.

The change in water wetting in the presence of n-heptane was reflected in the optical profilometry results shown in Figures 3(c) and (d). According to Figure 3(d), in a water/n-heptane system, the areas of the surface that were wet by the condensed water can be recognized by a deeper corrosion attack compared to adjacent areas that were covered by n-heptane and, therefore, were uncorroded. The profilometry map corroborates well with the SEM image in Figure 3(b). Note that, according to Figure 3(a), in the absence of n-heptane, the surface experienced a more uniform mode of corrosion. SEM images of the surface of specimen after the blank test (B), at low and high magnification (Figure 3[a]), show selective dissolution of ferrite and the remaining iron carbide (Fe<sub>3</sub>C) after corrosion. A few FeCO<sub>3</sub> crystals are also observed at high magnification.

Moving forward with the analysis of the behavior of inhibitors, in this discussion the experiments with inhibitors in water-only environments are compared to the wateronly blank experiment (B) while the experiments with inhibitors in water-heptane environments are compared to the blankheptane experiment (B-Hep). As shown in Figure 2 and Table 3, decanethiol was effective in decreasing the corrosion rate in the absence of the hydrocarbon phase. However, when n-heptane was added to the system, this inhibitor completely lost its IE (IE = 0%). This was evidenced by a higher corrosion rate under this condition, similar to the blank experiment with n-heptane. The maximum penetration rate, in the presence of decanethiol and n-heptane in the system, was also similar to the value obtained in the blank-heptane experiment, showing the loss of inhibition for decanethiol at this condition.

Hexanethiol, on the other hand, presented the opposite behavior. As depicted in Figure 2 and Table 3, in the experiment without a hydrocarbon phase, this inhibitor showed lower IE compared to decanethiol. This means in the water-only condensing environment, the IE increased with the alkyl tail length. These results are in agreement with those of Hosseinpour, et al., 20 who studied the effect of tail length of alkanethiols on the atmospheric corrosion mitigation of copper. According to their results, a higher level of packing and crystallinity of the absorbed layer of inhibitor on the surface with the longer tail length is expected. Such a layer impedes water, oxygen, and other corrosive species from reaching the metal surface, therefore protecting it from corrosion. Similar results in TLC experiments (similar to the current research) were reported by Belarbi, et al., who compared the IE of hexanethiol, decanethiol, and 11-mercaptoundecanoic acid applied to X65 carbon steel in an acidic CO2 environment and reported an increase in the IE with the alkyl tail length.

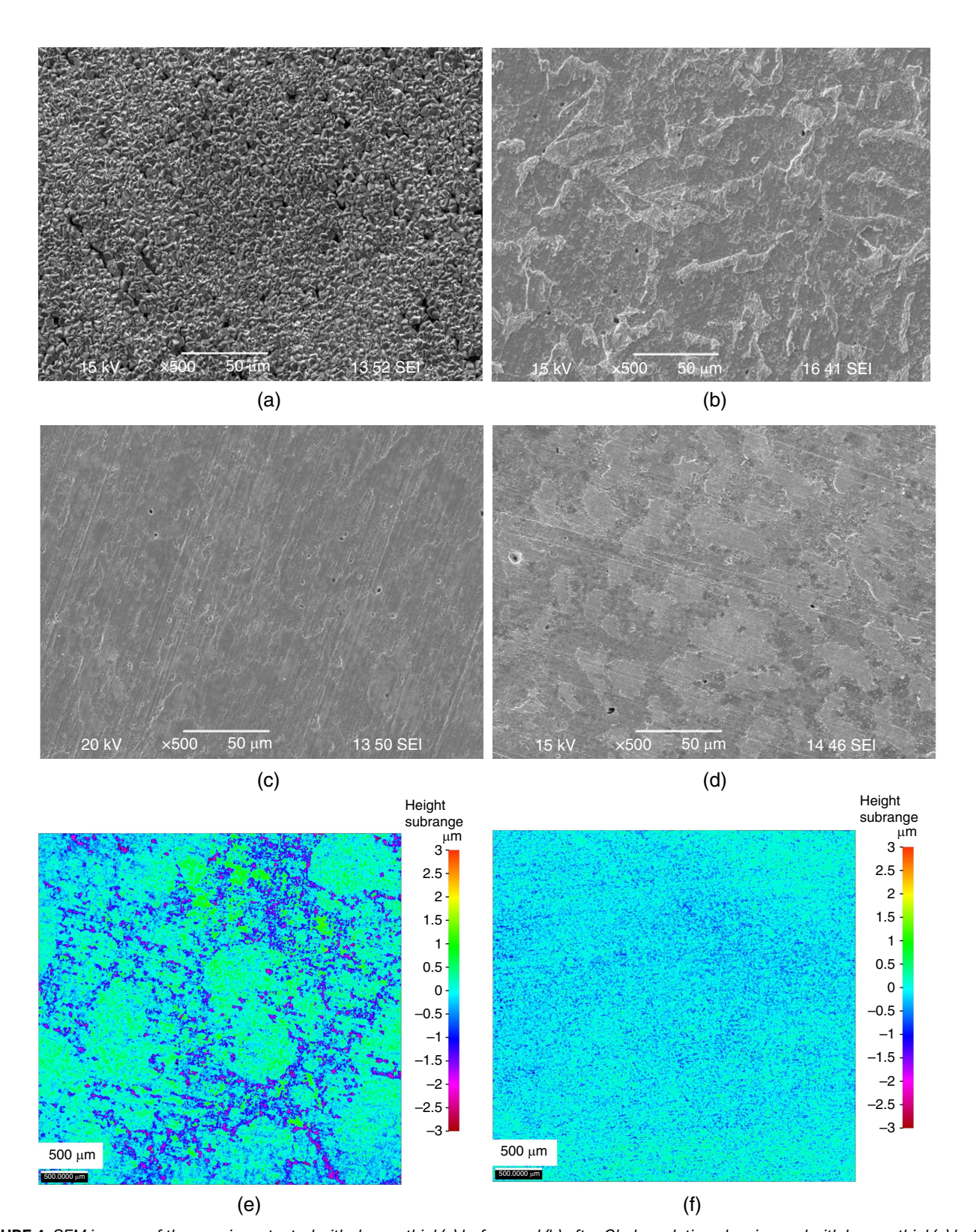
While this behavior of hexanethiol in  $CO_2$  saturated water was quite expected, its behavior in the water/n-heptane cocondensing environment was rather surprising. According to Figure 2 and Table 3, the presence of this inhibitor resulted in a reduction in the corrosion rate when the hydrocarbon phase was present in the system. At this condition, hexanethiol provided a higher IE compared to decanethiol. Before this behavior is discussed any further, results of surface characterization after each of the mentioned experiments require examination.

Figure 4 compares the SEM images and the optical profilometry data of the specimens tested with decanethiol

and hexanethiol in the presence of n-heptane in the system. Figure 4(a) shows that the surface of the specimen tested with decanethiol in a water/n-heptane system was covered by  $FeCO_3$  (on the entire surface as confirmed by images at lower magnification [not shown here]). The surface of the specimen tested with hexanethiol (under similar conditions) was free from any corrosion product. This difference can be due to a higher  $FeCO_3$  supersaturation stemming from the higher corrosion rate in the experiment with decanethiol. The results of EDS analysis for Figures 4(a) and (c) are shown in Figure 5 providing further confirmation of this observation. The O peak with relative high intensity in Figure 5(b) can indirectly indicate the formation of corrosion product layers (possibly  $FeCO_3$ ).

According to the SEM image of the surface after Clarke solution treatment (Figure 4[b]), the  $FeCO_3$  layer has formed following an initial high rate of corrosion. The morphology of the surface underneath this layer suggests the presence of  $Fe_3C$  residues. On the other hand, the surface of the specimen tested with hexanethiol clearly shows a less severe corrosion attack (Figure 4[d]). Similar to the SEM images, the results of optical profilometry confirm that, under these experimental conditions, corrosion was more uniform and maximum penetration was lower when hexanethiol was used (see Figures 4[e] and [f]).

The different corrosion behavior of specimens with decanethiol and hexanethiol during co-condensation of water and n-heptane can be attributed to their different solubility in water and n-heptane and the effect of solvent on the kinetics of adsorption. Researchers previously reported that the higher solubility of decanethiol in n-heptane compared to water leads to its partitioning in the hydrocarbon phase, both in the bottom solution and on the surface of the specimen. This partitioning results in the loss of IE.29 While this conclusion seems reasonable, the behavior of hexanethiol in n-heptane (with a similar solubility to that of decanethiol in n-heptane) indicates a more complex effect of the solvent. In 1996, Peterlinz and Georgiadis<sup>43</sup> studied the dependency of adsorption kinetics (with a gold substrate) on the solvent type, concentration, and tail length of alkanethiols. Their results showed that, in polar solvents such as ethanol (or water as in this study), the adsorption of alkanethiols on a gold substrate involved two kinetic steps. On the contrary, they observed that in a nonpolar solvent such as heptane, the adsorption (or the film growth) process consisted of a single step. According to Plimpton, 40 in a polar solvent (ethanol), the rate constant of the first step can be described equally well by both a diffusion-limited Langmuir adsorption model and a second order Langmuir adsorption model and it decreases with the tail length of alkanethiol, which is consistent with diffusion-limited kinetics. The rate constant in the second kinetic step which is slower and hence the rate-controlling step shows the opposite trend, meaning that film growth rates increase monotonically with increasing tail length. In a nonpolar solvent (heptane), kinetics of adsorption can be described by a single step Langmuir adsorption model and adsorption rate decreases with the tail length of alkanethiol.<sup>39</sup> This could mean that in polar solvents (such as water and ethanol), the adsorption kinetics increase with the tail length, while in nonpolar solvents (such as heptane) the adsorption kinetics decrease with the tail length. Despite the qualitative nature of this comparison, it could potentially explain why in water condensing environments, decanethiol (with a longer tail length hence faster adsorption kinetics) provides a better corrosion inhibition compared to hexanethiol (with a shorter tail length and a slower adsorption



**FIGURE 4.** SEM images of the specimen tested with decanethiol (a) before and (b) after Clarke solution cleaning and with hexanethiol (c) before and (d) after Clarke solution treatment. Optical profilometry analysis of the specimen tested with (e) decanethiol and (f) hexanethiol (both experiments contained n-heptane).

kinetics). The opposite behavior is observed in water/n-heptane co-condensing environments. It is important to note that the current study did not involve an adsorption kinetic analysis. Instead, a molecular simulation method was chosen to

elucidate the mechanism and the observed behavior, which will be detailed later in the manuscript.

It can be argued that the higher vapor pressure (6  $\times$  10<sup>-3</sup> bar vs. 8.2  $\times$  10<sup>-5</sup> bar at 25°C) and the higher molar concentration

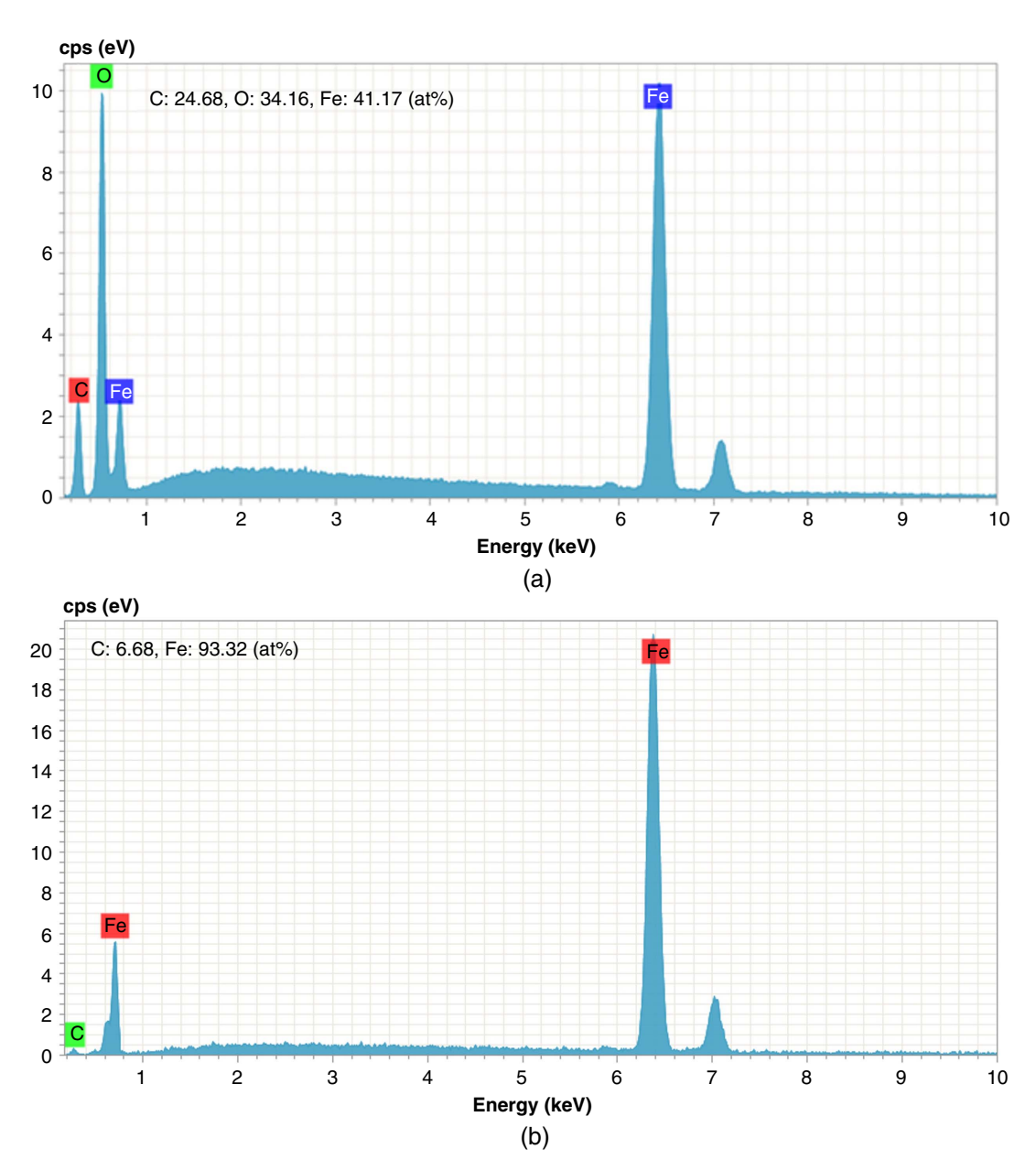


FIGURE 5. EDS spectra of the specimen tested with (a) decanethiol and (b) hexanethiol before Clarke solution cleaning (both experiments contained n-heptane).

of hexanethiol compared to decanethiol (at the same "ppm concentration") due to the smaller molar mass of hexanethiol compared to decanethiol (118.24 g/mol vs. 174.3 g/mol) can influence the adsorption kinetics. This argument is probably not valid because, first, the same behavior was not observed in a water-only condensing environment and, second, according to Peterlinz and Georgiadis<sup>43</sup> the adsorption kinetics are not dependent on the concentration of alkanethiols at high concentrations (higher than 10<sup>-6</sup> M). Therefore, even though decanethiol would provide a better protection efficiency in a hydrocarbon-free environment compared to hexanethiol, the abovementioned hypothesis can be postulated to explain the better protection efficiency conferred by hexanethiol in a co-condensing environment.

To better understand the impact of n-heptane on the corrosion IE of hexanethiol, molecular simulations were

performed. In these studies, the role of the size of the alkane on the synergistic adsorption behavior of the corrosion inhibitor was analyzed. Details of the model are discussed in the Molecular Simulations section. The hypothesis is that the adsorption of corrosion inhibitors is enhanced when the length of the alkane is similar to that of the alkyl tails of the inhibitor molecules. The rationale is that if the alkane is smaller, then it would either not play any role in the inhibitor adsorption or will disrupt the hydrophobic interactions between the alkyl tails of the inhibitors. On the other hand, if the alkane is long then the inhibitors will aggregate with the alkane molecules in the bulk phase rather than adsorbing on the surface. However, when the alkane is of commensurate length, then it will get incorporated in the adsorbed layer and strengthen the hydrophobic interactions between the alkyl tails. To test our hypothesis, the adsorption of a 20 bead long corrosion inhibitor without any

alkane molecules and in the presence of alkanes of length 10, 19, and 25 beads was studied.

Figure 6 shows the simulation results, where the adsorption density,  $\rho$  ( $\sigma^{-2}$ ) defined as the number of molecules per

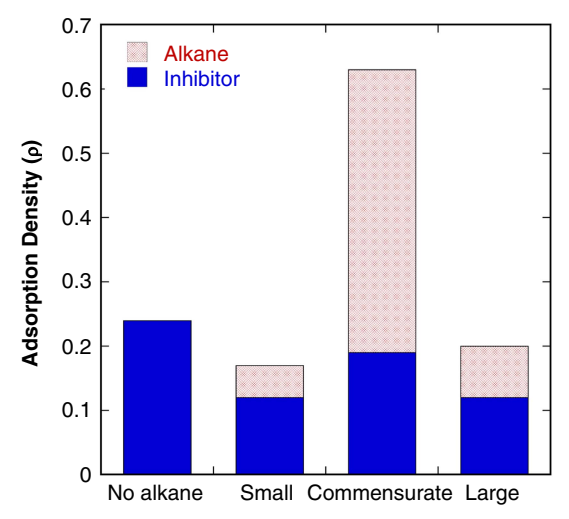


**FIGURE 6.** Adsorption density,  $\rho$  of inhibitor and alkane molecules in molecular simulations for the cases when there is no alkane, small (10 bead) alkane, alkane of size commensurate with the alkyl tail of the inhibitor (19 bead), and a large alkane (25 bead) in the system.

unit area is plotted. In the absence of any alkane in the system, the p was 0.24. In the presence of small (10 bead) alkane molecules, the adsorption was disrupted with  $\rho = 0.17$ with a small amount of alkane co-adsorbing with the inhibitor. When the alkane molecules were commensurate in size (19 bead), then the adsorption jumped to  $\rho = 0.63$ . It has been shown in previous work that this corrosion inhibitor model adsorbs in a cylindrical micelle morphology.37 The reason for this significant increase in the  $\rho$  is because a large number of alkane molecules get incorporated in the adsorbed layer and the overall adsorption morphology becomes planar.<sup>37</sup> Coadsorption of alkane molecules increases the hydrophobic character of the adsorbed film. In the presence of large (25 bead) alkane molecules, the ρ was 0.20. Therefore, longer alkanes also disrupted the adsorption tendency of the inhibitors. Figure 7 shows snapshots of the simulations with small, commensurate, and large alkanes. The system with commensurate alkanes showed synergistic adsorption between the alkanes and the inhibitors, which improved the adsorption. Small alkanes remained dispersed in the system and therefore did not improve the adsorption. Large alkanes had a strong tendency to aggregate amongst themselves in the bulk phase and thus did not help in the adsorption. These results verify our hypothesis and provide an explanation for the improvement in the IE manifested by hexanethiol in the presence of n-heptane.

It is well-known that commercial inhibitors comprise of several active, as well as inactive, from a corrosion inhibition

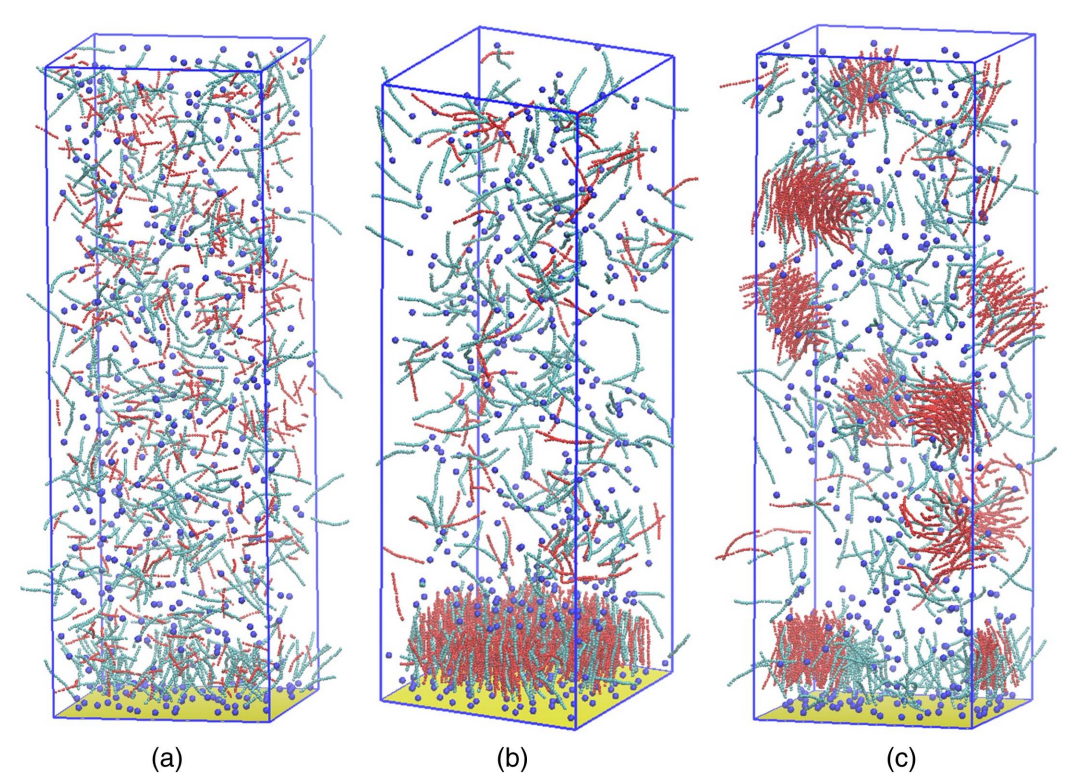


FIGURE 7. Snapshots of the simulation system with (a) small, (b) commensurate, and (c) large alkanes with corrosion inhibitors. Alkane molecules are represented by red color. Cyan color beads represent the alkyl tails of the inhibitors and blue beads represent the polar head groups. (b) Shows significantly more adsorption as compared to (a) and (c) with alkanes and inhibitor molecules co-adsorbing. Large alkanes (panel [c]) have a stronger tendency to aggregate amongst themselves in the bulk phase and therefore do not aid in the adsorption. Small alkanes (panel [a]) remain dispersed in the solution and therefore do not improve the adsorption.

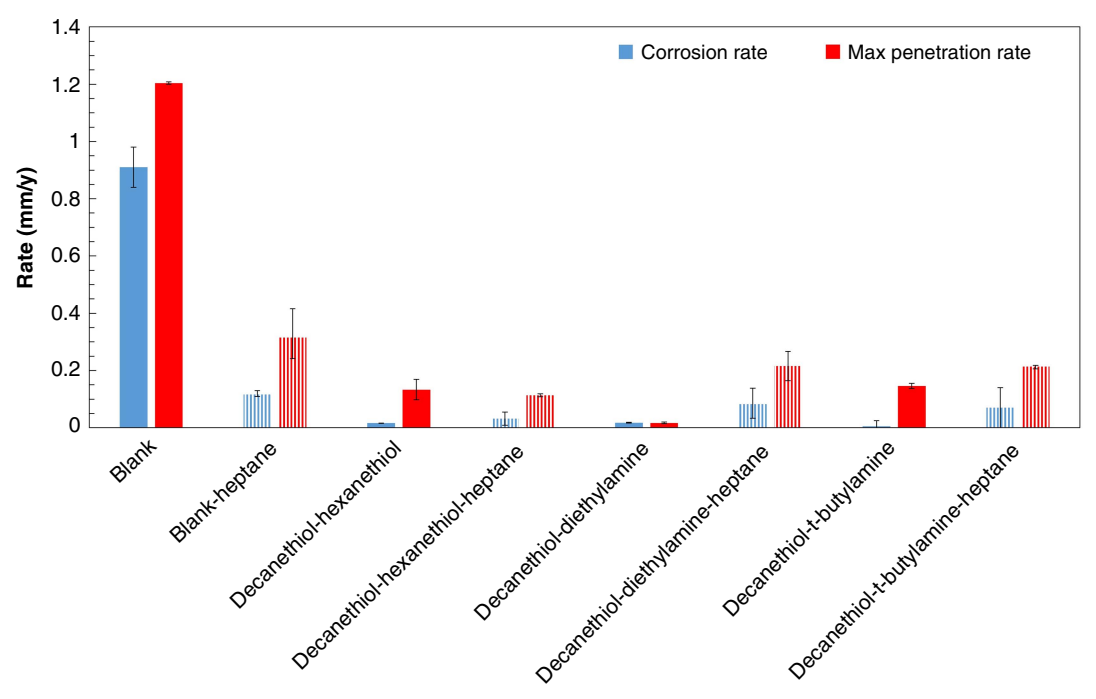


FIGURE 8. Results of corrosion rate for different TLC experiments with VCI mixtures (the error bars represent maximum and minimum values).

**Table 4.** IE for Various Inhibitor Mixtures Tested in this Study in Water-Only and Co-Condensing Environment of Water and n-Heptane

1. 1. 1. 1. 1. 1. 1. 1. 1. 1. 1. 1. 1. 1								
	Decanethiol- Hexanethiol/ Water	Decanethiol- Hexanethiol/ Water-Heptane	Decanethiol- Diethylamine/ Water	Decanethiol- Diethylamine/ Water-Heptane	Decanethiol-t- Butylamine/ Water	Decanethiol-t- Butylamine/ Water-Heptane		
IE (%)	98.2	72.7	98.1	29.5	99.5	39.8		

perspective, compounds. Therefore, additional experiments were performed to investigate if a mixture of inhibitor molecules could provide a synergistic effect in systems containing a condensable hydrocarbon phase. Figure 8 shows the corrosion rate and maximum penetration rate obtained from three different mixtures of inhibitors in environments with and without hydrocarbon (n-heptane). The results of the blank experiments are also included in this graph for comparison. The tested mixtures included decanethiol/hexanethiol, decanethiol/diethylamine, and decanethiol/t-butylamine.

Table 4 summarizes the results of IE for the mixture of inhibitors tested in this study in the presence and absence of n-heptane.

The results shown in Figure 8 and Table 4 indicate that when the specimen was tested with a mixture of two thiols (decanethiol and hexanthiol), notable corrosion mitigation was observed in the condensed water environment. Under this condition, both corrosion rate and the maximum penetration rate were significantly decreased. Indeed, in the absence of n-heptane, this mixture of inhibitors showed a lower corrosion rate compared to decanethiol. It is unlikely that this behavior is due to the higher concentration of inhibitor in this experiment (400 ppm decanethiol and 400 ppm hexanethiol),

mostly because of the independence of adsorption kinetics on the concentration of inhibitor at high concentrations.<sup>43</sup> It is suspected that the observed phenomenon could be related to a higher level of packing of the adsorbed layer. Unlike decanethiol, the mentioned mixture did not lose its IE when exposed to co-condensing environments. This behavior was most probably due to the presence of hexanethiol in the mixture that, as mentioned earlier, showed a high IE in the presence of n-heptane.

Figure 9 depicts the surface of the specimens tested with a mixture of decanethiol and hexanethiol both in the presence and absence of n-heptane in the system. The two specimens showed similar surfaces protected from corrosion with no accumulation of corrosion products (Figures 9[a] and [c]). In both cases, the polishing marks (from the preparation step) were still visible on the surface of the specimens. Despite observing initial stages of corrosion on the surfaces, no signs of significant localized corrosion (Figures 9[b] and [d]) were observed after treatment with Clarke solution.

According to the results in Table 4, in the condensed water environment, the mixture of decanethiol and diethylamine and the mixture of decanethiol and t-butylamine show a remarkably high IE with a corrosion rate  $\leq 0.01$  mm/y. Under this condition, the maximum penetration rate for both mixtures

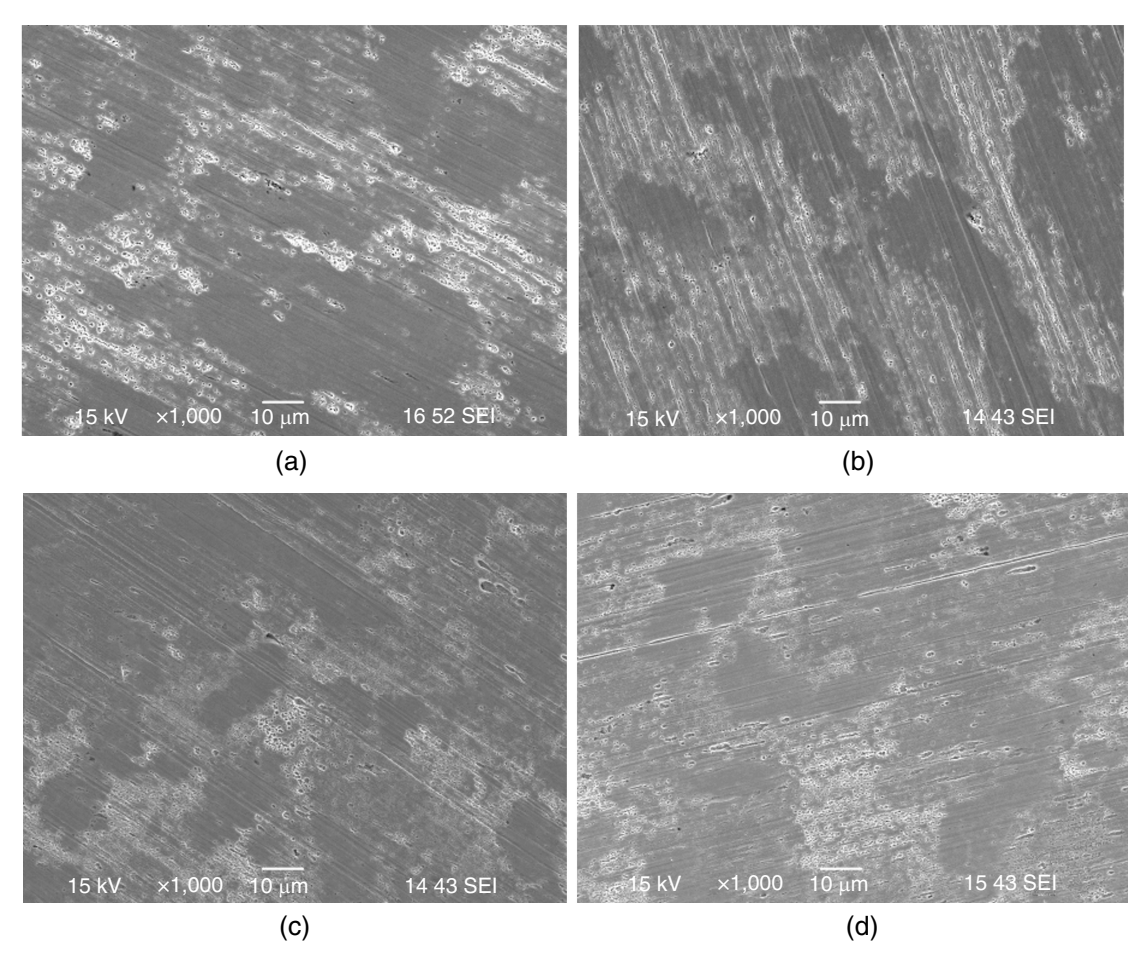


**FIGURE 9.** SEM image of the specimen after the experiment with decanethiol-hexanethiol (a) before and (b) after Clarke solution cleaning and with decanethiol-hexanethiol (with n-heptane) (c) before and (d) after Clarke solution cleaning.

was  $\leq$  0.15 mm/y, similar to that of the mixture of decanethiol and hexanethiol. While amines were previously shown to be ineffective in preventing corrosion under similar experimental conditions,  $^{26}$  the results of this study clearly demonstrate that their synergistic effect with decanethiol is promising. The corrosion and maximum penetration rates obtained with these two mixtures were the lowest among all of the cases studied herein. This could be partly due to the increase in pH of the solution as a result of amine protonation, which decreases the corrosion rate. For example, if comparisons are made between the pH of the bottom solution in the experiment D-Di (4.68±0.04) to that of D-H (3.64±0.04) and also the pH of condensed water in the experiment D-Di (3.90±0.06) to that of D-H (3.80±0.05), the effect of addition of amine on the pH is observed.

SEM images of the surface of specimens tested with these mixtures confirm their high IE. According to the SEM images in Figure 10, no corrosion product and no localized corrosion were visible on the surface before or after cleaning with Clarke solution. The surface of all specimens showed the polishing marks from the specimen preparation step and minimal corroded features.

Table 4 also shows that when the mixture of decanethiol and diethylamine and the mixture of decanethiol and t-butylamine were tested under co-condensation conditions, their IE was

significantly reduced. More specifically, according to Figure 8, a maximum penetration rate of ca. 0.2 mm/y was observed. This rate was higher than the rate obtained after the experiments with the same mixtures but under water-only condensation condition (ca. 0.01 mm/y to ca. 0.1 mm/y) and was similar to that of the blank-heptane experiment.

The SEM images of specimens tested under cocondensation conditions (Figures 11[a] and [b]), that were taken after removing the corrosion product layer, show severe corrosion in both cases. This means that the mixtures of thiol and amines lost their IE in the presence of the hydrocarbon phase in the system.

As explained earlier, the kinetics of adsorption of decanthiol are slower in the presence of n-heptane compared to the water-only condensing environment and, therefore, this inhibitor cannot provide a high IE in co-condensing environments. On the other hand, while the two used amines have a lower molecular mass compared to decanethiol and can potentially increase the kinetics of film formation, their concentration in the bulk solution (and subsequently in the condensed water) is reduced due to the acidic environment and protonation. This means that unlike hexanethiol, the addition of amines cannot compensate for the poor IE of decanethiol in water/hydrocarbon co-condensing scenarios. The optical profilometry maps of the tested surfaces

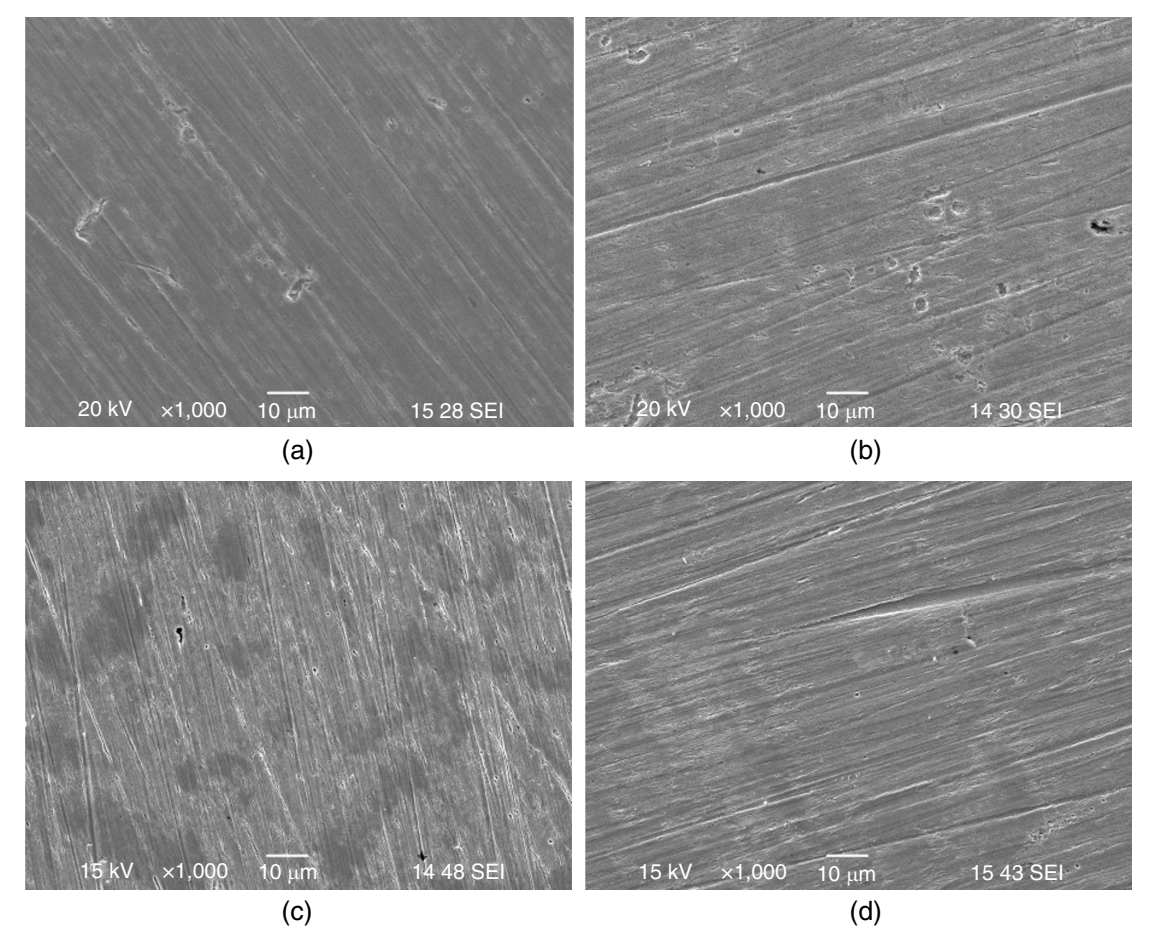
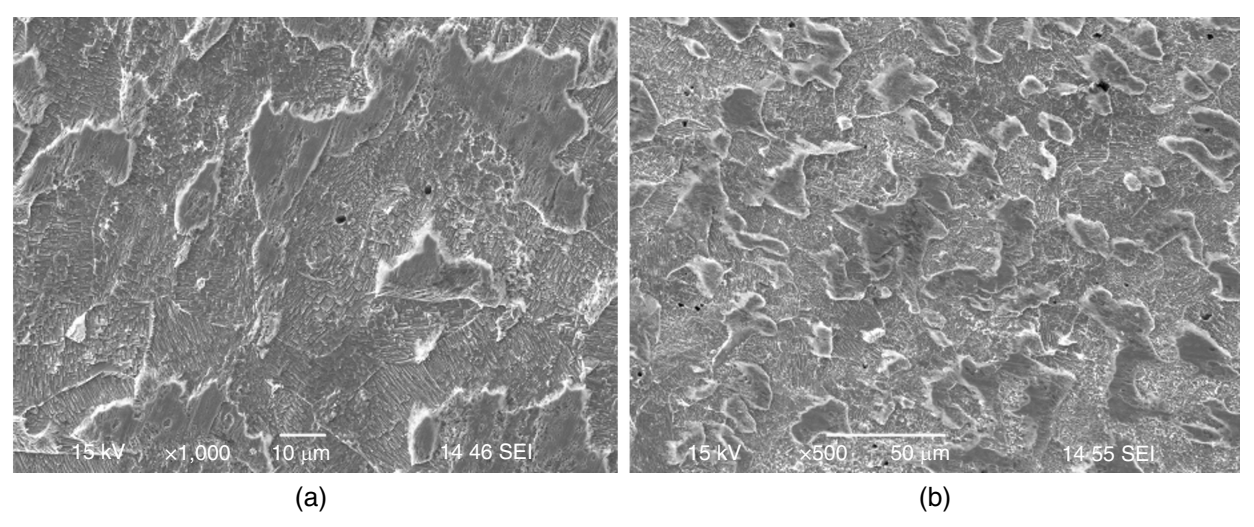


FIGURE 10. SEM image of the specimen after the experiment with decanethiol-diethylamine (a) before and (b) after Clarke solution cleaning and with decanethiol-t-butylamine (c) before and (d) after Clarke solution cleaning.



**FIGURE 11.** SEM image of the specimen after the experiment with (a) decanethiol-diethylamine and (b) decanethiol-t-butylamine (both experiments contained n-heptane, SEM images taken after Clarke solution cleaning).

(D-Di-Hep and D-t-B-Hep) in Figures 12(a) and (b) confirm the presence of localized corrosion features in both cases.

These results undermine the premise of the synergistic inhibiting effect of decanethiol and amines, in the presence of a condensable hydrocarbon phase. However, further

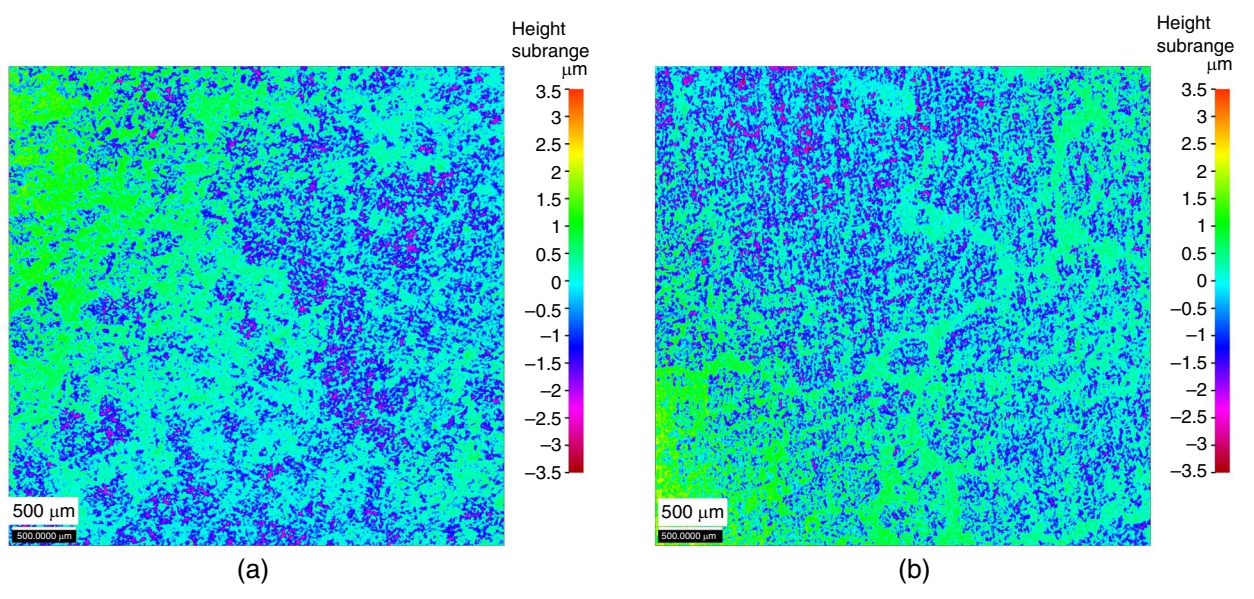


FIGURE 12. Optical profilometry analysis of the specimen after the test with (a) decanethiol-diethylamine and (b) decanethiol-t-butylamine (both experiments contained n-heptane).

experiments are needed to determine the IE of the mixture of hexanethiol and amines.

#### CONCLUSIONS

The following conclusions can be drawn from this study: > The presence of a condensable hydrocarbon phase (n-heptane) interfered with the IE of the studied model VCIs and their mixtures, except for hexanethiol and the decanethiol/hexanethiol mixture.

- > Decanethiol provided 94% corrosion IE in the condensed water environment but lost its efficiency in co-condensation conditions (0% IE).
- > Hexanethiol provided a better corrosion inhibition in co-condensation scenarios with n-heptane compared to decanethiol (81% vs. 0% efficiency)
- > Molecular simulation results showed that in the presence of alkanes of commensurate size with the inhibitor's alkyl tails, a synergistic adsorption occurred, where alkane molecules got incorporated with the inhibitors thereby increasing the adsorbed amount and the hydrophobic character of the adsorbed film.
- > The mixture of thiols with different alkyl tail lengths provided corrosion IE higher than 70% in the presence and absence of the hydrocarbon phase.
- > The mixture of decanethiol and amines did not provide any improved corrosion protection for TLC scenarios in the presence of the hydrocarbon phase.
- > The use of thiols with alkyl tail of similar lengths to those of the alkane of the hydrocarbon phases present in the environment of application can improve the IE of mixture of inhibitors in co-condensing scenarios.

## **ACKNOWLEDGMENTS**

Financial support from the following companies is greatly appreciated: MI-Swaco, PTTEP, Shell, Saudi Aramco, and Arkema. Sumit Sharma thanks the support from the National Science Foundation (NSF) CAREER grant 2046095 and the NSF ACCESS grant DMR190005 for computational resources.

#### References

- M. Singer, "Top-of-the-Line Corrosion," in *Trends in Oil and Gas Corrosion Research and Technologies*, ed. A.M. El-Sherik (Boston, MA: Woodhead Publishing, 2017), p. 385-408.
- M. Singer, D. Hinkson, Z. Zhang, H. Wang, S. Nešić, Corrosion 69, 7 (2013): p. 719-735.
- M. Nordsveen, S. Nešić, R. Nyborg, A. Stangeland, Corrosion 59, 5 (2003): p. 443-456.
- Z. Belarbi, T.N. Vu, F. Farelas, D. Young, M. Singer, S. Nešić, Corrosion 73, 7 (2017): p. 892-899.
- T. Pojtanabuntoeng, M. Eslami, M. Singer, S. Nešić, Corrosion 78, 4 (2022): p. 295-306.
- G. Schmitt, M. Scheepers, G. Siegmund, "Inhibition of the Top-ofthe-Line Corrosion under Stratified Flow," CORROSION 2001, paper no. 01032 (Houston, TX: NACE, 2001).
- Y.M. Gunaltun, A. Belghazi, "Control of Top of the Line Corrosion by Chemical Treatment," CORROSION 2001, paper no. 01033 (Houston, TX: NACE, 2001).
- 8. M. Pan, K.S. Bahadori, M. Eslami, B. Brown, M. Singer, "Development of Methodologies for Continuous and Batch Inhibitor Film Persistency Investigation in the Laboratory," CORROSION 2022, paper no. 18056 (Houston, TX: AMPP, 2022).
- J. Yang, V. Jovancicevic, S. Mancuso, J. Mitchell, "High Performance Batch Treating Corrosion Inhibitor," CORROSION 2007, paper no. 07693 (Houston, TX: NACE, 2007).
- R.L. Martin, "Control of Top-of-Line Corrosion in a Sour Gas Gathering Pipeline with Corrosion Inhibitors," CORROSION 2009, paper no. 09288 (Houston, TX: NACE, 2009).
- A. Subramanian, M. Natesan, V.S. Muralidharan, K. Balakrishnan, T. Vasudevan, Corrosion 56, 2 (2000): p. 144-155.
- 12. B. Boyle, Met. Finish. 102, 5 (2004): p. 37-41.
- D.M. Bastidas, E. Cano, E. Mora, *Anti-Corros. Methods Mater.* 52, 2 (2005): p. 71-77.
- I.L. Rosenfeld, B.P. Persiantseva, P.B. Terentiev, Corrosion 20, 7 (2013): p. 222t-234t.
- Z. Belarbi, J.M.D. Olivo, F. Farelas, M. Singer, D. Young, S. Nešić, *Corrosion* 75, 10 (2019): p. 1246-1254.
- T. Kawai, H. Nishihara, K. Aramaki, J. Electrochem. Soc. 143, 12 (1996): p. 3866.
- 17. M.A. Quraishi, D. Jamal, Corrosion 58, 5 (2002): p. 387-391.
- 18. J. Rawat, M.A. Quraishi, Corrosion 59, 3 (2003): p. 238-241.
- Y. Feng, W.K. Teo, K.S. Siow, Z. Gao, K.L. Tan, A.K. Hsieh, J. Electrochem. Soc. 144, 1 (1997): p. 55.
- S. Hosseinpour, C.M. Johnson, C. Leygraf, J. Electrochem. Soc. 160, 6 (2013): p. C270.

- 21. M. Ehteshamzadeh, T. Shahrabi, M. Hosseini, *Anti-Corros. Methods Mater.* (2006): p. 296-302.
- 22. S. Hosseinpour, M. Göthelid, C. Leygraf, C.M. Johnson, *J. Electrochem. Soc.* 161, 1 (2014): p. C50.
- F.-I. Xu, J.-d. Yang, R. Qiu, J. Hou, J.-y. Zheng, J.-w. Zhang, L. Wang,
   Z.-y. Sun, C.-g. Lin, *Prog. Org. Coat.* 97 (2016): p. 82-90.
- M.C. Folena, J.A. Da Cunha Ponciano Gomes, I. Manfield, H.A. Farhat, J. Owen, A. Neville, R. Barker, "Residual Analysis Assay for Thiol-Based Volatile Corrosion Inhibitor Quantification in Topof-Line Corrosion Environments," CORROSION 2022, paper no. 17918 (Hosuton, TX: AMPP, 2022).
- E. Cano, D.M. Bastidas, J. Simancas, J.M. Bastidas, *Corrosion* 61, 5 (2005): p. 473-479.
- Z. Belarbi, F. Farelas, M. Singer, S. Nešić, *Corrosion* 72, 10 (2016): p. 1300-1310
- S. Nasrazadani, J. Diaz, J. Stevens, R. Theimer, Corros. Sci. 49, 7 (2007): p. 3024-3039.
- X. Zhang, Y.T. Ma, Y. Li, M.K. Lei, F.H. Wang, Corrosion 69, 7 (2013): p. 647-654.
- Z. Belarbi, F. Farelas, D. Young, M. Singer, S. Nešić, "Effect of Operating Parameters on the Inhibition Efficacy of Decanethiol," CORROSION 2018, paper no. 10823 (Houston, TX: NACE, 2018).
- 30. A. Rafefi, Corrosion 78, 8 (2022): p. 799-810.
- U. Rammelt, S. Koehler, G. Reinhard, Corrosion 67, 4 (2011): p. 045001-045007.

- 32. T. Pojtanabuntoeng, "Influence of Water/Hydrocarbons Co-Condensation on Top of the Line Corrosion" (PhD Thesis, Ohio University, 2012).
- 33. ASTM G1-03, "Standard Practice for Preparing, Cleaning, and Evaluating Corrosion Test Specimens" (West Conshohocken, PA: ASTM International, 2011).
- 34. ASTM G31 21, "Standard Guide for Laboratory Immersion Corrosion Testing of Metals" (West Conshohocken, PA: ASTM International, 2004).
- 35. W. Zhang, B. Brown, D. Young, G. Bota, S. Nešić, M. Singer, *Corros. Sci.* 183 (2021): p. 109305.
- 36. X. Ko, S. Sharma, J. Phys. Chem. B 121, 45 (2017): p. 10364-10370.
- 37. X. Ko, J. Dominguez Olivo, B. Brown, S. Nešić, S. Sharma, *Corrosion* 76, 11 (2020).
- 38. X. Ko, S. Sharma, J. Phys. Chem. B 124, 26 (2020): p. 5517-5524.
- S. Sharma, H. Singh, X. Ko, J. Phys. Chem. B 123, 34 (2019): p. 7464-7470.
- 40. S. Plimpton, J. Comput. Phys. 117, 1 (1995): p. 1-19.
- T. Pojtanabuntoeng, M. Singer, S. Nešić, "Water/Hydrocarbon Co-Condensation and the Influence on Top-of-the -Line Corrosion," CORROSION 2011, paper no.11330 (Houston, TX: NACE, 2011).
- V. Fajardo, M. Eslami, Y.-S. Choi, B. Brown, S. Nešić, Corrosion 77, 1 (2021): p. 97-111.
- 43. K.A. Peterlinz, R. Georgiadis, *Langmuir* 12, 20 (1996): p. 4731-4740.